Inorg. Chem. **2007**, *46*, 2002–2010

Tuned Triazolatesilver(I) Luminescent Complexes from Zero- to Three-Dimensionality Based on Bi- to Tetratopic Bridged Ligands

Ying Wang, Bin Ding, Peng Cheng,* Dai-Zheng Liao, and Shi-Ping Yan

Department of Chemistry, Nankai University, Tianjin 300071, People's Republic of China

Received May 17, 2006

The self-assembly of silver(I) salts with bitopic triazole ligands 4-(salicylideneamino)-1,2,4-triazole (L_1) and 4-(2-pyridinyl)-1,2,4-triazole (L_2) produced dinuclear complexes and a 1D molecular-ladder coordination polymer, while the reaction of tritopic ligand 4-(3-pyridinyl)-1,2,4-triazole (L_3) with $AgClO_4$ afforded a right-handed helical 2D network with (4,4) topology, a meso layer constructed via left- and right-handed helical chains with $AgBF_4$, and a 2D 4.8^2 net containing no helical chain with $AgNO_3$. Using a tetratopic triazole ligand 2,6-bis(4-triazolyl)pyridine (L_4), a 3D coordination polymer was isolated. This complex contains a cationic 4.6^3 network with rhombic channels, accepting two columns of uncoordinated ClO_4^- anions filling into every central cavity. Our results show that (i) the increase of coordination sites of the ligands is an effective route to obtaining higher-dimensional structures and (ii) anions could influence the configuration of the ligand to tune the coordination network topology from those with helical chains to those without. In the solid state, all of the complexes exhibit strong fluorescent emission bands, which may be assigned to intraligand fluorescent emission. The luminescent properties of these complexes in a water solution varied from blue light to green light at ambient temperature.

Introduction

The current topical areas focus on the construction of metal−organic frameworks (MOFs) with novel topology and on the crystal engineering of molecular architectures organized by coordination bonds and supramolecular contacts (such as hydrogen bonding, $\pi-\pi$ interactions, etc.).[1−3] Thus, many spectacular MOFs have been documented, such as 1D chains[4] and ladders,[5] 2D grids,[6] 3D microporous networks,[7] interpenetrated modes,[8] and helical staircase networks,[9] which show promise in new materials, such as molecular magnets, optoelectronic devices, sensors, catalysts, and so on.[10] Considerable efforts have been made on the theoretical prediction and control of the topologies of coordination

* To whom correspondence should be addressed. E-mail: pcheng@nankai.edu.cn.

(1) (a) Chui, S. S.-Y.; Lo, S. M.-F.; Charmant, J. P. H.; Orphen, A. G.; Williams, I. D. *Science* **1999**, *283*, 1148. (b) Seo, J.-S.; Whang, D.; Lee, H.; Jun, S. I.; Oh, J.; Jeon, Y. J.; Kim, K. *Nature* **2000**, *404*, 982.

(2) (a) Moulton, B.; Zaworotko, M. J. *Chem. Rev.* **2001**, *101*, 1629. (b) Evans, O. R.; Lin, W. B. *Acc. Chem. Res.* **2002**, *35*, 511.

(3) (a) Fu, A. H.; Huang, X. Y.; Li, J.; Yuen, T.; Lin, C. L. *Chem.−Eur. J.* **2002**, *8*, 2239. (b) Zhao, B.; Cheng, P.; Dai, Y.; Cheng, C.; Liao, D. Z.; Yan, S. P.; Jiang, Z. H.; Wang, G. L. *Angew. Chem., Int. Ed.* **2003**, *42*, 934. (c) Zhao, B.; Chen, X. Y.; Cheng, P.; Liao, D. Z.; Yan, S. P.; Jiang, Z. H. *J. Am. Chem. Soc.* **2004**, *126*, 15394. (d) Kasai, M.; Aoyagi, M.; Fujita, M. *J. Am. Chem. Soc.* **2000**, *122*, 2140. (e) Kitaura, R.; Seki, K.; Akiyama, G.; Kitagawa, S. *Angew. Chem., Int. Ed.* **2003**, *42*, 428.

(4) (a) Yi, L.; Yang, X.; Cheng, P.; Lu, T. B. *Cryst. Growth Des.* **2005**, *5*, 1215. (b) Gao, H.-L.; Yi, L.; Zhao, B.; Zhao, X.-Q.; Cheng, P.; Liao, D.-Z.; Yan, S.-P. *Inorg. Chem.* **2006**, *45*, 5980.

(5) (a) Withersby, M. A.; Blake, A. J.; Champness, N. R.; Cooke, P. A.; Hubberstey, P.; Li, W. S.; Schröder, M. *Inorg. Chem.* **1999**, *38*, 2259. (b) Chen, B.; Fronczek, F. R.; Maverick, A. W. *Inorg. Chem.* **2004**, *43*, 8209. (c) Papaefstathiou, G. S.; Georgiev, I. G.; Friščić, T.; MacGillvray, L. R. *Chem. Commun.* **2005**, 3974.

(6) (a) Mitsurs, K.; Shimamura, M.; Noro, S. I.; Minakoshi, S.; Asami, A.; Seki, K.; Kitagawa, S. *Chem. Mater.* **2000**, *12*, 1288. (b) Zhang, L.; Cheng, P.; Tang, L.-F.; Jiang, Z.-H.; Liao, D.-Z.; Yan, S.-P.; Wang, G.-L.; Weng, L.-H. *Chem. Commun.* **2000**, 717.

(7) (a) Pan, L.; Sander, M. B.; Huang, X.; Li, J.; Smith, M.; Bittner, E.; Bockrath, B.; Johnson, J. K. *J. Am. Chem. Soc.* **2004**, *126*, 1308. (b) Wu, C.-D.; Lin, W. *Chem. Commun.* **2005**, 3673. (c) Xiang, S.; Wu, X.; Zhang, J.; Fu, R.; Hu, S.; Zhang, X. *J. Am. Chem. Soc.* **2005**, *127*, 16352.

(8) (a) Hill, R. J.; Long, D.-L.; Champness, N. R.; Hubberstey, P.; Schröder, M. *Acc. Chem. Res.* **2005**, *38*, 335. (b) Nattinen, K. I.; Rissanen, K. *Inorg. Chem.* **2003**, *42*, 5126. (c) Kostakis, G. E.; Casella, L.; Hadjiliadis, N.; Monzani, E.; Kourkoumelis, N.; Plakatouras, J. C. *Chem. Commun.* **2005**, 3859.

(9) (a) Maggard, P. A.; Stern, C. L.; Poeppelmeier, K. R. *J. Am. Chem. Soc.* **2001**, *123*, 7742. (b) Prabhakar, M.; Zacharias, P. S.; Das, S. K. *Inorg. Chem.* **2005**, *44*, 2585. (c) Anokhina, E. V.; Jacobson, A. J. *J. Am. Chem. Soc.* **2004**, *126*, 3044.

(10) (a) Fujita, M.; Kwon, Y. J. *J. Am. Chem. Soc.* **1994**, *116*, 1151. (b) Berlinguette, C. P.; Dragulescu-Andrasi, A.; Sieber, A.; Galan-Mascaros, J. R.; Gudel, H.-U.; Achim, C.; Dunbar, K. R. *J. Am. Chem. Soc.* **2004**, *126*, 6222. (c) Leadbeater, N. E.; Marco, M. *Chem. Rev.* **2002**, *102*, 3217. (d) Tsuchida, E.; Oyaizu, K. *Coord. Chem. Rev.* **2003**, *237*, 213. (e) Tsukube, H.; Shinoda, S. *Chem. Rev.* **2002**, *102*, 2389.

10.1021/ic060855y CCC: $37.00
Published on Web 02/10/2007

networks to produce useful functional materials,[11] and some successes have been reported. Most investigations in this area have used rigid ligands because they allow a better prediction of the overall structure, shape, and porosity of the resulting array. Actually, a plethora of interactions (e.g., $\pi-\pi$ interactions, metal−metal interactions, metal−π interactions) besides covalent metal−ligand contacts have an influence on the outcome of the resulting supramolecular array.[12] The culmination of all of the studies has led to the principles that can be applied in the design of new structures with a high degree of confidence.

Previously, we reported a series of triazolatecadmium(II) coordination polymers with different coordination modes tuned via different triazole ligands and anions.[13] Also, the luminescent properties of the ligands and organic−inorganic coordination polymers in the solid state and in a water solution were explored. In the context of increasing structural dimensionality and imparting intriguing photoluminescent characteristics to metal-containing assemblies, silver(I) is a favorable building block for constructing MOFs because of its flexible coordination numbers and weak metal−metal or metal−ligand interactions.[14] Herein, a systematic study of 4-(salicylideneamino)-1,2,4-triazole (L_1), 4-(2-pyridinyl)-1,2,4-triazole (L_2), 4-(3-pyridinyl)-1,2,4-triazole (L_3), and 2,6-bis(4-triazolyl)pyridine (L_4) with AgX salts (X = ClO_4^-, BF_4^-, NO_3^-) was performed. The important and potentially attractive aspect of this contribution is the fact that the ligands (L_2-L_4) being used are luminescent, thereby giving potential functionality (such as small-molecule sensing by fluorescence quenching) to these MOFs.

Experimental Section

Materials. The triazole ligands were synthesized according to the literature method.[15] All other reagents were commercially available and used without further purification. The C, H, and N microanalyses were carried out with a Perkin-Elmer 240 elemental analyzer. The photoluminescence spectrum was measured by a MPF-4 fluorescence spectrophotometer with a xenon arc lamp as the light source. Powder X-ray diffraction (PXRD) measurements were recorded on a D/Max-2500 X-ray diffractometer using Cu Kα radiation. Thermal analyses (under an oxygenated atmosphere with a heating rate of 5 °C min^{-1}) were carried out in a Labsys NETZSCH TG 209 Setaram apparatus. Electrospray ionization mass spectrometry (ESI-MS) spectra were obtained with a Sciex Qstar Pulsar and the ESI source. The UV−vis spectra were obtained on a Jasco V-570 spectrophotometer.

Caution! *Although no problems were encountered in this study, transition-metal perchlorate complexes are potentially explosive and should be handled with proper precautions.*

Preparations. Synthesis of $[Ag_2(\mu_2\text{-}L_1)_2(CH_3CN)_2](ClO_4)_2$ (1a), $[Ag_2(\mu_1\text{-}L_1)_2(\mu_2\text{-}L_1)_2](BF_4)_2\cdot 2H_2O$ (1b), and $[Ag_2(\mu_1\text{-}L_1)_2(\mu_2\text{-}L_1)_2](NO_3)_2$ (1c). Complexes **1a**−**1c** were prepared by the reaction of L_1 (0.3 mmol) and AgX (0.3 mmol; X = ClO_4^- for **1a**, BF_4^- for **1b**, and NO_3^- for **1c**) in a H_2O/CH_3CN (1:1) solution. After stirring for about 20 min, the resulting solution was filtered. Colorless single crystals suitable for X-ray diffraction were obtained by slow evaporation of the solvents in the dark within 7 days. Complex **1a**. Yield: 65%. Anal. Calcd for $C_{11}H_{11}AgClN_5O_5$ (436.57): C, 30.26; H, 2.54; N, 16.04. Found: C, 30.59; H, 2.63; N, 15.92. UV−vis (DMF, λ_{max}): 269, 332 nm. Complex **1b**. Yield: 68%. Anal. Calcd for $C_{18}H_{18}AgBF_4N_8O_3$ (589.08): C, 36.70; H, 3.08; N, 19.02. Found: C, 36.96; H, 2.86; N, 19.45. UV−vis (DMF, λ_{max}): 269, 340 nm. Complex **1c**. Yield: 55%. Anal. Calcd for $C_{18}H_{16}AgN_9O_5$ (546.27): C, 39.58; H, 2.95; N, 23.08. Found: C, 39.79; H, 2.77; N, 23.42. UV−vis (DMF, λ_{max}): 276, 334 nm.

Synthesis of $\{[Ag_4(\mu_2\text{-}L_2)_6(H_2O)(ClO_4)](ClO_4)_3\cdot H_2O\cdot 1.5CH_3CN\}_n$ (2a) and $[Ag_2(\mu_1\text{-}L_2)_2(\mu_2\text{-}L_2)_2](BF_4)_2$ (2b). Complexes **2a** and **2b** were prepared by the reaction of L_2 (0.3 mmol) and AgX (0.3 mmol; X = ClO_4^- for **2a** and BF_4^- for **2b**) in a H_2O/CH_3CN (1:1) solution. After stirring for about 20 min, the resulting solution was filtered. Colorless single crystals suitable for X-ray diffraction were obtained by slow evaporation of the solvents in the dark within 7 days. Complex **2a**. Yield: 52%. Anal. Calcd for $C_{45}H_{44.5}Ag_4Cl_4N_{25.5}O_{18}$ (1803.84): C, 29.96; H, 2.49; N, 19.80. Found: C, 29.65; H, 2.12; N, 19.51. UV−vis (DMF, λ_{max}): 270 nm. Complex **2b**. Yield: 45%. Anal. Calcd for $C_{28}H_{24}Ag_2B_2F_8N_{16}$ (973.99): C, 34.53; H, 2.48; N, 23.01. Found: C, 34.32; H, 2.55; N, 23.36. UV−vis (DMF, λ_{max}): 270, 290 nm.

Synthesis of $\{[Ag_2(\mu_3\text{-}L_3)_2(CH_3CN)](ClO_4)_2\}_n$ (3a), $\{[Ag(\mu_3\text{-}L_3)]BF_4\}_n$ (3b), and $\{[Ag(\mu_3\text{-}L_3)]NO_3\cdot H_2O\}_n$ (3c). Complexes **3a**−**3c** were prepared by the reaction of L_3 (0.3 mmol) and AgX (0.3 mmol; X = ClO_4^- for **3a**, BF_4^- for **3b**, and NO_3^- for **3c**) in a H_2O/CH_3CN (1:1) solution. After stirring for about 20 min, the resulting solution was filtered. Colorless single crystals suitable for X-ray diffraction were obtained by slow evaporation of the solvents in the dark within 7 days. Complex **3a**. Yield: 61%. Anal. Calcd for $C_{16}H_{15}Ag_2Cl_2N_9O_8$ (748.01): C, 25.69; H, 2.02; N, 16.85. Found: C, 25.41; H, 1.93; N, 17.05. UV−vis (DMF, λ_{max}): 270, 430 nm. Complex **3b**. Yield: 72%. Anal. Calcd for $C_7H_6AgBF_4N_4$ (340.84): C, 24.67; H, 1.77; N, 16.44. Found: C, 24.96; H, 1.86; N, 16.75. UV−vis (DMF, λ_{max}): 270, 440 nm. Complex **3c**. Yield: 46%. Anal. Calcd for $C_7H_8AgN_5O_4$ (334.05): C, 25.17; H, 2.41; N, 20.97. Found: C, 25.26; H, 2.19; N, 20.65. UV−vis (DMF, λ_{max}): 268 nm.

Synthesis of $\{[Ag(\mu_4\text{-}L_4)]ClO_4\}_n$ (4). Complex **4** was prepared by the reaction of L_4 (0.3 mmol) and $AgClO_4$ (0.3 mmol) in a H_2O/CH_3CN (1:1) solution. After stirring for about 20 min, the resulting solution was filtered. Colorless single crystals suitable for X-ray diffraction were obtained by slow evaporation of the solvents in the dark within 7 days. Yield: 73%. Anal. Calcd for $C_9H_7AgClN_7O_4$ (420.54): C, 25.71; H, 1.68; N, 23.32. Found: C, 25.58; H, 1.46; N, 23.44. UV−vis (DMF, λ_{max}): 265, 310 nm.

Crystal Structure Determination. Single-crystal X-ray diffraction measurements of the title complexes were carried out on an APEX II CCD area detector equipped with a graphite crystal monochromator situated in the incident beam for data collection at 293(2) K. The structures were solved by direct methods and refined with full-matrix least-squares techniques using the *SHELXS-97* and

(11) Kasai, M.; Aoyagi, M.; Fujita, M. *J. Am. Chem. Soc.* **2000**, *122*, 2140.
(12) (a) Khlobystov, A. N.; Blake, A. J.; Champness, N. R.; Lemenovskii, D. A.; Majouga, G.; Zyk, N. V.; Schroder, M. *Coord. Chem. Rev.* **2001**, *222*, 155. (b) Blake, A. J.; Champness, N. R.; Hubberstey, P.; Li, W. S.; Withersby, M. A.; Schröder, M. *Coord. Chem. Rev.* **1999**, *183*, 117.
(13) (a) Yi, L.; Ding, B.; Zhao, B.; Cheng, P.; Liao, D.-Z.; Yan, S.-P.; Jiang, Z.-H. *Inorg. Chem.* **2004**, *43*, 33. (b) Ding, B.; Yi, L.; Wang, Y.; Cheng, P.; Liao, D.-Z.; Yan, S.-P.; Jiang, Z.-H. *Dalton Trans.* **2006**, 665. (c) Huang, Y.-Q.; Ding, B.; Song, H.-B.; Zhao, B.; Ren, P.; Cheng, P.; Wang, H.-G.; Liao, D.-Z.; Yan, S.-P. *Chem. Commun.* **2006**, 4906.
(14) (a) Wilkinson, G. *Comprehensive Coordination Chemistry*; Pergamon Press: New York, 1987. (b) Wang, Y.; Yi, L.; Yang, X.; Ding, B.; Cheng, P.; Liao, D.-Z.; Yan, S.-P. *Inorg. Chem.* **2006**, *45*, 5822.
(15) Wiley, R. H.; Hart, A. J. *J. Org. Chem.* **1953**, *18*, 1368.

Table 1. Crystallographic Data and Details of Refinements for Complexes **1a**−**1c**, **2a**, and **2b**

	1a	**1b**	**1c**	**2a**	**2b**
empirical formula	$C_{11}H_{11}AgClN_5O_5$	$C_{18}H_{18}AgBF_4N_8O_3$	$C_{18}H_{16}AgN_9O_5$	$C_{45}H_{44.5}Ag_4Cl_4N_{25.5}O_{18}$	$C_{28}H_{24}Ag_2B_2F_8N_{16}$
M	436.57	589.08	546.27	1803.84	973.99
cryst syst	monoclinic	triclinic	triclinic	triclinic	triclinic
space group	*C*2/*m*	$P\bar{1}$	$P\bar{1}$	$P\bar{1}$	$P\bar{1}$
a/Å	20.014(2)	9.0524(14)	7.8128(18)	14.676(4)	9.259(6)
b/Å	6.4738(8)	10.0477(16)	10.954(3)	15.821(4)	11.977(8)
c/Å	11.5786(14)	14.264(2)	13.092(3)	15.985(4)	16.373(11)
α/deg	90	90.998(2)	70.034(2)	68.894(3)	89.136(9)
β/deg	91.574(2)	108.058(2)	74.568(3)	67.259(3)	77.588(8)
γ/deg	90	115.308(2)	86.273(3)	87.049(4)	81.274(8)
V/Å^3	1499.6(3)	1098.0(3)	1014.7(4)	3176.8(14)	1752(2)
Z	4	2	2	2	2
cryst size/mm	0.34 × 0.17 × 0.10	0.39 × 0.25 × 0.16	0.42 × 0.16 × 0.12	0.36 × 0.15 × 0.12	0.34 × 0.19 × 0.07
D_c/g cm^{-3}	1.934	1.782	1.788	1.886	1.846
μ/mm^{-1}	1.556	0.992	1.048	1.472	1.209
F(000)	864	588	548	1786	960
θ range/deg	1.76−25.03	2.28−25.03	1.71−25.03	1.88−25.03	1.72−25.03
total data	4116	5946	5529	17410	9535
unique data	1456	3806	3554	11091	6096
R_{int}	0.0162	0.0176	0.0129	0.0264	0.0178
R1[a] [$I > 2\sigma(I)$]	0.0487	0.0331	0.0249	0.0500	0.0370
wR2[a] [$I > 2\sigma(I)$]	0.1538	0.0812	0.0726	0.1356	0.1068
S[b]	1.166	1.057	1.075	1.019	1.059

[a] $R1(F_o) = \sum||F_o| - |F_c||/|F_o|$, $wR2(F_o^2) = [\sum w(F_o^2 - F_c^2)^2/\sum w(F_o^2)^2]^{1/2}$. [b] $S = \{\sum[w(F_o^2 - F_c^2)^2]/(n - p)\}^{1/2}$.

Table 2. Crystallographic Data and Details of Refinements for Complexes **3a**−**3c** and **4**

	3a	**3b**	**3c**	**4**
empirical formula	$C_{16}H_{15}Ag_2Cl_2N_9O_8$	$C_7H_6AgBF_4N_4$	$C_7H_8AgN_5O_4$	$C_9H_7AgClN_7O_4$
M	748.01	340.84	334.05	420.54
cryst syst	monoclinic	monoclinic	monoclinic	monoclinic
space group	*P*2(1)/*n*	*P*2(1)/*n*	*C*2/*c*	*P*2(1)/*n*
a/Å	15.777(2)	9.341(2)	10.5853(16)	4.8700(8)
b/Å	8.2118(11)	7.9006(18)	13.746(2)	18.833(3)
c/Å	18.983(2)	14.698(3)	14.809(2)	13.780(2)
α/deg	90	90	90	90
β/deg	98.442(2)	97.987(3)	103.151(3)	93.757(2)
γ/deg	90	90	90	90
V/Å^3	2432.8(5)	1074.2(4)	2098.2(5)	1261.1(4)
Z	4	4	8	4
cryst size/mm	0.42 × 0.31 × 0.18	0.28 × 0.12 × 0.08	0.26 × 0.18 × 0.10	0.31 × 0.21 × 0.09
D_c/g cm^{-3}	2.042	2.108	2.115	2.215
μ/mm^{-1}	1.892	1.912	1.934	1.844
F(000)	1464	656	1312	824
θ range/deg	2.61−25.03	2.44−25.03	2.47−25.01	2.16−25.01
total data	12633	5626	5246	7233
unique data	4289	1900	1853	2228
R_{int}	0.0231	0.0167	0.0236	0.0186
R1[a] [$I > 2s(I)$]	0.0308	0.0329	0.0458	0.0348
wR2[a] [$I > 2\sigma(I)$]	0.0955	0.0965	0.1199	0.0968
S[b]	0.977	1.071	1.186	1.134

[a] $R1(F_o) = \sum||F_o| - |F_c||/|F_o|$, $wR2(F_o^2) = [\sum w(F_o^2 - F_c^2)^2/\sum w(F_o^2)^2]^{1/2}$. [b] $S = \{\sum[w(F_o^2 - F_c^2)^2]/(n - p)\}^{1/2}$.

SHELXL-97 programs.[16] Anisotropic thermal parameters were assigned to all non-H atoms. The H atoms of **1c** and **3c** were placed in idealized positions, while the H atoms of other complexes were placed in idealized positions and located in the difference Fourier map. The H atoms of water molecules in **1b** were found in the difference Fourier map. Analytical expressions of neutral-atom scattering factors were employed, and anomalous dispersion corrections were incorporated. The crystallographic data and selected bond lengths and angles for the title complexes are listed in Tables 1−3, respectively.

CCDC nos. 266098 (**1a**), 266101 (**1b**), 602554 (**1c**), 602179 (**2a**), 266088 (**2b**), 266099 (**3a**), 266096 (**3b**), 602553 (**3c**), and 266095 (**4**) contain the supplementary crystallographic data for this paper. These data can be obtained free of charge via www.ccdc.can.ac.uk/conts/retrieving.html (or from the Cambridge Crystallographic Data Centre, 12 Union Rd., Cambridge CB2 1EZ, U.K., fax (+44) 1223-336033, e-mail deposit@ccdc.cam.ac.uk).

(16) (a) Sheldrick, G. M. *SHELXL-97, Program for the Solution of Crystal Structures*; University of Göttingen: Göttingen, Germany, 1997. (b) Sheldrick, G. M. *SHELXL-97, Program for the Refinement of Crystal Structures*; University of Göttingen: Göttingen, Germany, 1997.

Results and Discussion

Synthesis of the Complexes. The 4-substituted 1,2,4-triazole ligands employed in this work are ditopic (L_1 and L_2), tritopic (L_3), and tetratopic (L_4), respectively, which are shown in Chart 1. Slow evaporation of the solvents at room temperature afforded either discrete compounds or coordination polymers and networks depending on the ligand and anion, as summarized in Scheme 1. The self-assembly of $AgClO_4$, $AgBF_4$, or $AgNO_3$ with ditopic triazole ligand L_1

Table 3. Selected Bond Lengths (Å) and Angles (deg) for the Title Complexes[a]

		Complex **1a**			
Ag1−N4	2.173(5)	Ag1−N3#1	2.356(6)	Ag1−N5	2.195(8)
N4−Ag1−N5	156.8(3)	N5−Ag1−N3#1	94.1(2)	N4−Ag1−N3#1	109.2(2)
		Complex **1b**			
Ag1−N5	2.197(2)	Ag1−N4	2.242(2)	Ag1−N3#1	2.283(3)
N5−Ag1−N4	132.54(9)	N4−Ag1−N3#1	108.67(9)	N5−Ag1−N3#1	118.49(10)
		Complex **1c**			
Ag1−N3	2.2253(19)	Ag1−N5	2.3242(19)	N6#1−Ag1−N5	110.66(7)
N6#1−Ag1−N3	127.35(7)				
		Complex **2a**			
Ag1−N22	2.235(5)	Ag1−N17	2.261(5)	Ag2−N14	2.174(5)
Ag1−N18#1	2.310(6)	Ag3−N13	2.367(5)	Ag2−N7	2.419(5)
Ag4−N4#2	2.327(5)	Ag3−N21	2.239(5)	N22−Ag1−N17	134.7(2)
N14−Ag2−N11	151.84(19)	N22−Ag1−N18#1	112.61(19)	N17−Ag1−N18#1	110.51(19)
N11−Ag2−N7	89.96(18)	N12−Ag4−O1′#2	87.4(2)	N12−Ag4−N4#2	99.18(18)
N14−Ag2−N7	117.29(18)	N8−Ag3−N21	133.9(2)	N3−Ag4−O1′#2	105.8(2)
N8−Ag3−N13	118.08(19)	N21−Ag3−N13	99.39(19)	N3−Ag4−N4#2	113.08(18)
N13−Ag3−O1′	90.4(2)	N3−Ag4−N12	138.2(2)		
		Complex **2b**			
Ag2−N14	2.359(4)	Ag2−N5	2.215(4)	Ag2−N10	2.201(4)
Ag1−N13	2.197(4)	Ag1−N6	2.331(4)	N10−Ag2−N5	137.41(14)
Ag1−N2	2.202(4)	N13−Ag1−N2	143.05(13)	N2−Ag1−N6	102.21(12)
N10−Ag2−N14	107.99(13)	N5−Ag2−N14	114.13(13)	N13−Ag1−N6	114.21(13)
		Complex **3a**			
Ag1−N4	2.240(3)	Ag1−N5	2.291(3)	Ag2−N6	2.221(3)
Ag1−N1#2	2.404(3)	Ag2−N9	2.177(4)	N9−Ag2−N3	113.55(14)
N5−Ag1−N8#1	108.07(11)	N5−Ag1−N1#2	104.54(10)	N6−Ag2−N3	114.93(11)
N4−Ag1−N5	114.28(10)	N4−Ag1−N8#1	127.08(10)	N9−Ag2−N6	130.94(13)
		Complex **3b**			
Ag1−N3	2.197(4)	N3−Ag1−N4#2	112.23(14)	Ag1−N4#2	2.313(4)
N3−Ag1−N1#1	135.15(14)	N1#1−Ag1−N4#2	112.56(13)	Ag1−N1#1	2.248(4)
		Complex **3c**			
Ag1−N2#1	2.255(5)	Ag1−N1	2.259(5)	Ag1−N4#2	2.264(5)
N2#1−Ag1−N1	115.07(18)	N2#1−Ag1−N4#2	120.64(19)	N1−Ag1−N4#2	121.92(17)
		Complex **4**			
Ag1−N7	2.237(3)	Ag1−N6#1	2.297(3)	Ag1−N1#3	2.581(4)
Ag1−N2#2	2.325(3)	N6#1−Ag1−N1#3	122.25(12)	N7−Ag1−N2#2	133.50(13)
N7−Ag1−N1#3	89.56(12)	N6#1−Ag1−N2#2	97.03(12)	N7−Ag1−N6#1	113.95(11)

[a] Symmetry transformations used to generate equivalent atoms. For **1a**: #1, $-x+1, -y, -z+2$. For **1b**: #1, $-x+1, -y+1, -z$. For **1c**: #1, $-x, -y-1, -z+2$. For **2a**: #1, $-x+1, -y+2, -z+1$; #2, $-x+2, -y+2, -z+1$. For **3a**: #1, $-x+{}^3/_2, y-{}^1/_2, -z+{}^1/_2$; #2, $-x+{}^5/_2, y+{}^1/_2, -z+{}^1/_2$. For **3b**: #1, $x+{}^1/_2, -y+{}^1/_2, z-{}^1/_2$; #2, $-x+1, -y, -z$. For **4**: #1, $-x+2, -y+1, -z+2$; #2, $x+{}^3/_2, -y+{}^3/_2, z+{}^1/_2$; #3, $x+{}^1/_2, -y+{}^3/_2, z+{}^1/_2$.

Chart 1

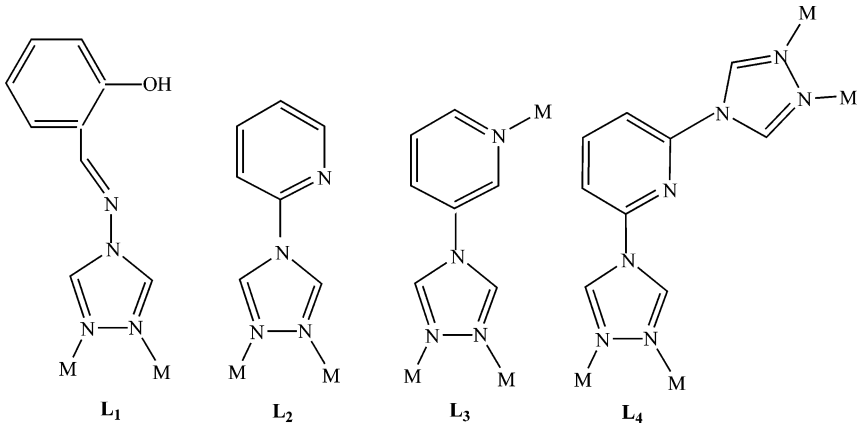

or L_2, dinuclear complexes **1a**−**1c** and **2b**, and a 1D molecular-ladder coordination polymer **2a** were obtained. Reactions of different silver(I) salts with L_3 yield three complexes with different structures. The right-handed helical 2D network **3a** with (4,4) topology, a meso layer **3b** constructed via left- and right-handed helical chains, and a 2D 4.8^2 net **3c** containing no helical chain have been afforded. Using L_4, a 3D coordination polymer **4** was isolated, which contains a cationic 4.6^3 network with rhombic channels, accepting two columns of uncoordinated ClO_4^-

Scheme 1

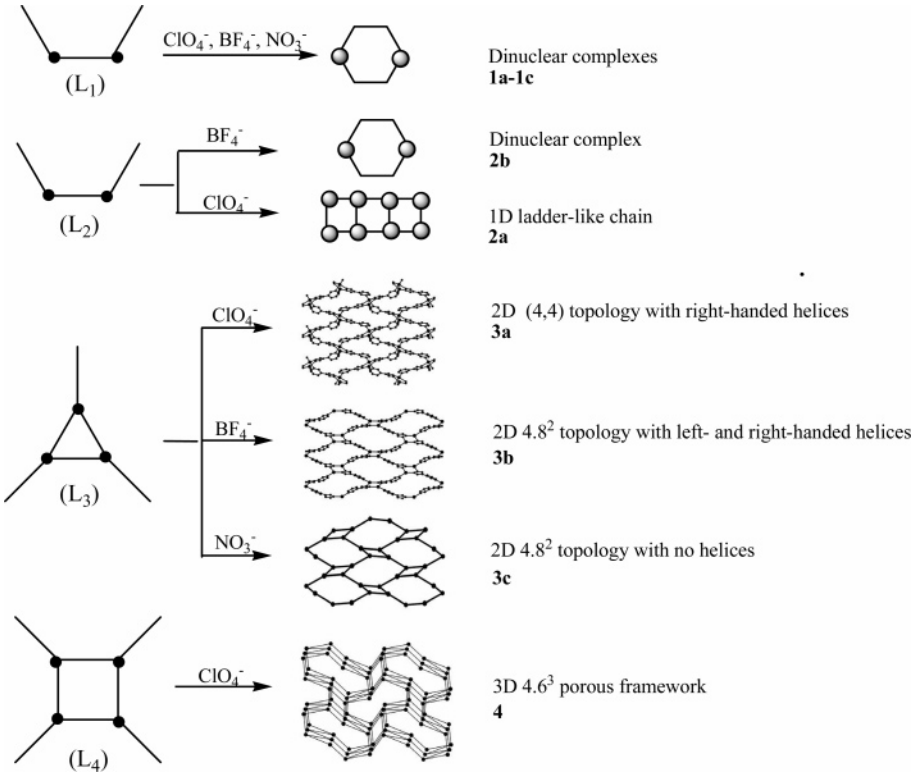

anions. The complexes were characterized in the solid state by single-crystal PXRD and emission spectroscopy and in solution by other methods as detailed below.

General Characterization. All of the title complexes are only fairly soluble in water but can be dissolved in H_2O/CH_3CN and *N*,*N*-dimethylformamide (DMF). UV−vis spectra of all of the title complexes in DMF have been measured (see the Supporting Information). The strong bands about 270 nm for all of the complexes can be attributed to intraligand absorption. ESI-MS measurements demonstrate that both the dinuclear complex **2b** and the 2D coordination polymer **3b** decomposed into monomeric structures in DMF. In the MS spectrum, the observed peaks in the positive MS spectrum are *m*/*z* 341.04 for **2b** and *m*/*z* 340.94 for **3b**, which correspond to $[Ag(L_2)(DMF)]^+$ and $[Ag(L_3)(DMF)]^+$, respectively (see the Supporting Information). All of the above assignments were confirmed by good agreements between the observed and calculated isotopic distributions.

Thermogravimetric analyses (TGA) of **3a** and **3b** were performed to investigate the thermal stability of the coordination frameworks (see the Supporting Information). The first weight loss of **3a** between 140 and 162 °C is 5.1%because of the loss of CH_3CN molecules (5.5%). The facile removal of CH_3CN molecules confirms that the coordination interactions among the CH_3CN molecules and Ag^I cations are relatively weak. The decomposition of the coordination networks is at 300 and 260 °C for **3a** and **3b**, respectively. The behaviors of TGA and differential thermal analysis curves imply that the decompositions of the coordination networks in **3a** and **3b** are similar. Finally, complete decomposition of both compounds is not achieved until 600 °C.

Structural Analysis of 1a−1c. 1a features a Ag_2 dimer, with each Ag^I center bonding to two $N_{triazole}$ atoms and one $N_{acetonitrile}$ atom. Ag1 and Ag1A (A = $-x + 1$, $-y$, $-z + 2$) are bridged by two L_1 ligands to form a six-membered ring $\{Ag_2N_4\}$. The Ag···Ag separation is 4.01 Å, which is significantly longer than the sum of the van der Waals radii of two Ag atoms (3.44 Å).[14a] All of the atoms in **1a** are fairly coplanar. When $AgBF_4$ and $AgNO_3$ were employed, dinuclear complexes **1b** and **1c** were afforded. Compared with **1a**, two L_1 in **1b** and **1c** act as terminal ligands instead of acetonitrile molecules (Figure 1). The dihedral angle formed between the aromatic and triazole rings is in the range of 6.6−16.4°, indicating that they are nearly coplanar in L_1. The above results show that the hydroxy group of L_1 does not coordinate with Ag^I in **1a**−**1c** and L_1 only acts as a bitopic ligand to construct discrete molecules.

Structural Analysis of 2a and 2b. As shown in Figure 2a, single-crystal X-ray determination indicates that L_2 in complex **2a** is a N1,N2-bridged motif to link Ag2 and Ag3 by double bridges or Ag1, Ag3 and Ag2, Ag4 by single bridges. Water molecules and perchlorate anions also act as bridges to link Ag1, Ag3 and Ag2, Ag4 in **2a**. As a result, a unique 1D molecular-ladder coordination chain is formed (Figure 3a). The hydrogen bonds connect such a 1D chain into a 3D supramolecular network (see the Supporting Information).

In **2b**, the dinuclear cation consists of both terminal and bridged bitopic L_2 ligands (Figure 2b), which have configurations similar to those in **1b** and **1c**. Two dinuclear cations in **2b** exist face-to-face supported via relatively strong $\pi-\pi$ interactions between aromatic rings (3.51−3.63 Å) of L_2

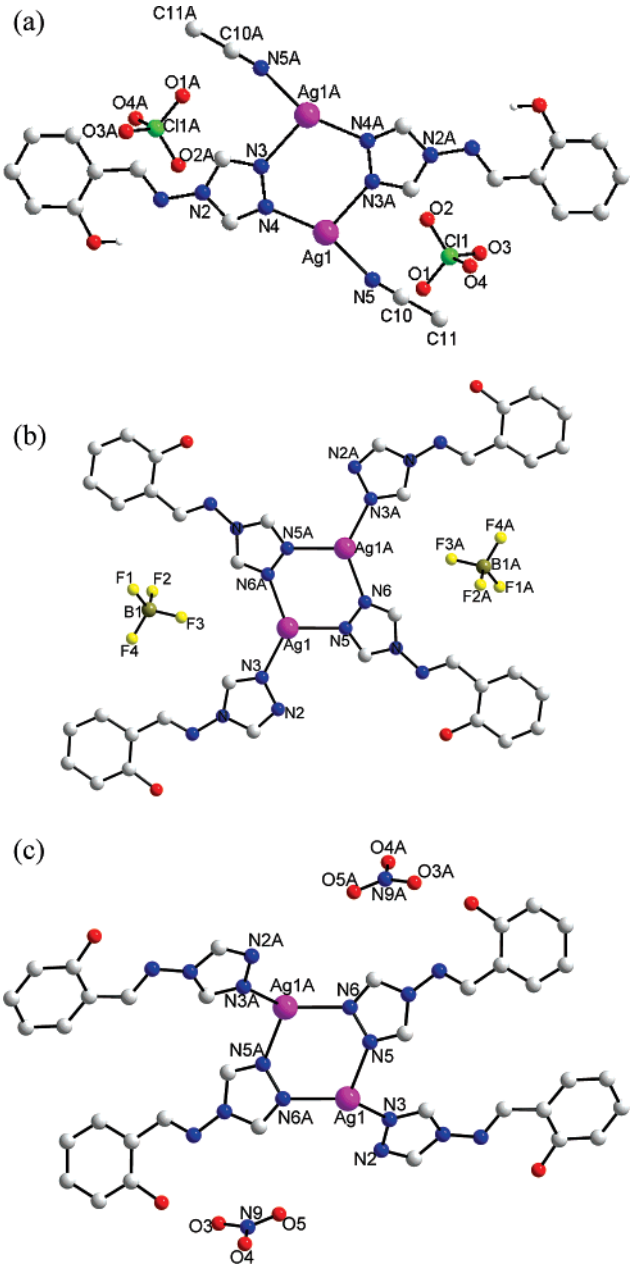

Figure 1. Dinuclear structures of **1a** (a), **1b** (b), and **1c** (c). Color code: purple, Ag; blue, N; red, O; gray, C; brown, B; yellow, F; white, H; green, Cl.

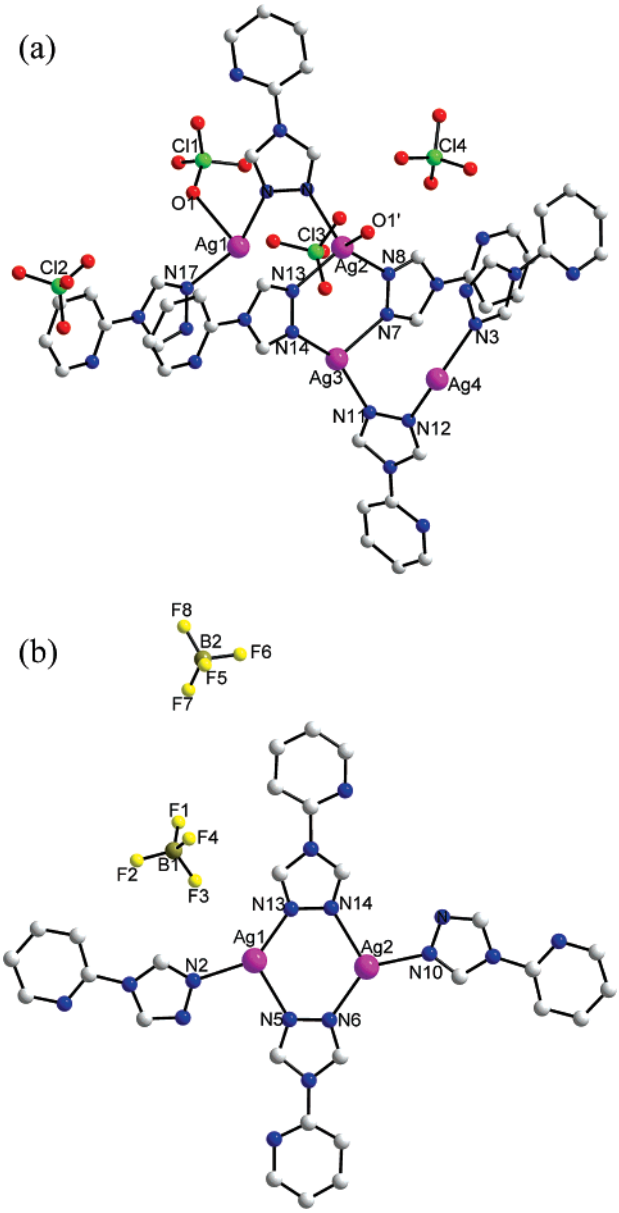

Figure 2. Coordination unit of **2a** (a) and dinuclear structure of **2b** (b). Color code: purple, Ag; blue, N; red, O; gray, C; brown, B; yellow, F; green, Cl.

ligands, constructing a supramolecular tetranuclear unit (Figure 3b). Interligand C−H···N hydrogen bonding interactions organize the dimers into polymeric chains in the *ab* direction and pyridyl C−H···F interactions organize these chains into 2D sheets. C−H···F interactions in conjunction with short Ag−π interactions and weak Ag···Ag contacts organize the sheets in the third dimension and form a 3D supramolecular network (see the Supporting Information). From the structural point of view, it is suggested that not only anions but also solvents play a key role in dictating the final structures.

Structural Analysis of 3a−3c. L_3 ligands act as three-connected nodes to coordinate with three Ag^I ions; as a result, three 2D coordination networks based on different silver(I) salts were isolated for **3a**−**3c**.

As shown in Figure 4a, there are three- and four-coordinated Ag^I centers bridged by two N1,N2-bridged L_3 ligands in each independent crystallographic unit for **3a**. The coordination environment around Ag1 is completed via two $N_{triazole}$ and two $N_{pyridine}$ atoms of four L_3 ligands. One acetonitrile molecule coordinates with the Ag2 center and two $N_{triazole}$ atoms. For **3a**, L_3 links each Ag1 center to form a cationic 2D grid network with (4,4) topology, in which the Ag^I atoms are in the same plane. Each L_3 ligand also links the Ag2 centers, which exist above and below the 2D (4,4) layer. The dihedral angles formed between the pyridine and triazole rings in L_3 are 24.8 and 37.7°, indicating a strong spatial distortion effect. Another unique structural feature of **3a** is that the homochiral right-handed helix is in an orderly arrangement and Ag1 atoms act as hinges (Figure 5). The pitch of each helix is 8.21 Å. The 2D layers are packed in an *ABAB* sequence, and there are no open channels

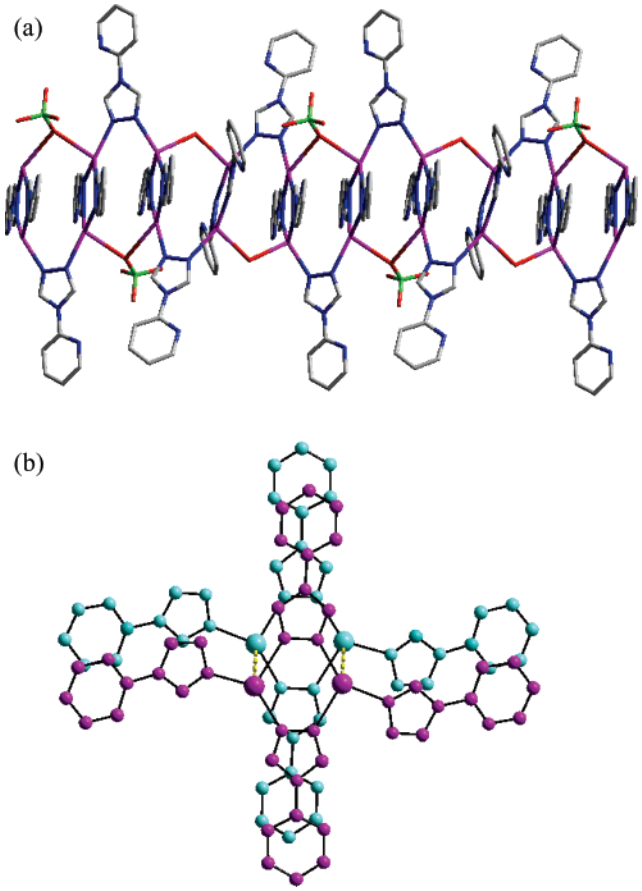

Figure 3. 1D molecular ladder of **2a** (a). Color code: purple, Ag; red, O; green, Cl; blue, N; gray, C. Double dinuclear units in **2b** (b). Yellow dashed line: Ag···Ag weak interaction.

in **3a**. Perchlorate anions exist between 2D layers, which weakly coordinate to Ag2 ions with Ag···O distances of 2.94 Å.

In **3b**, each Ag^I center is in a distorted triangular coordination comprised of three N donors from three distinct L_3 ligands (Figure 4b), which is similar to that in **3c**. **3b** is a 2D coordination polymer containing cationic layers with left- and right-handed helical chains (Figure 4c) and BF_4^- anions. For each μ_3-bridged L_3 ligand, the dihedral angle formed between the pyridine and triazole rings is 33.9°. At first sight, in the cationic layer, each ligand bridges two adjacent three-coordinated Ag^I centers to form twisted rectangular macrometallacycles $Ag_4(L_3)_4$, and such a repeating unit is extended along the *a* and *c* directions to form a 2D network (Figure 6). The ligands link Ag^I centers to form left- and right-handed helical chains. The pitch of both the left- and right-handed helices is 7.90 Å. Then alternately left- and right-handed helical chains are further bridged by Ag−N bonds to form a 2D meso layer. Each layer is parallel to the neighboring one, and the adjacent layers possess large channels with approximate dimensions of 16.6 × 7.4 Å.

The Ag^I centers in **3b** and **3c** have similar coordination environments but different configurations for the L_3 ligands (see the Supporting Information). As a result, they produce different 2D coordination networks. The crystal structure of **3c** shows that each L_3 ligand binds three Ag^I ions to form a 2D-layered motif with a 4.8^2 net organized by four L_3 ligands

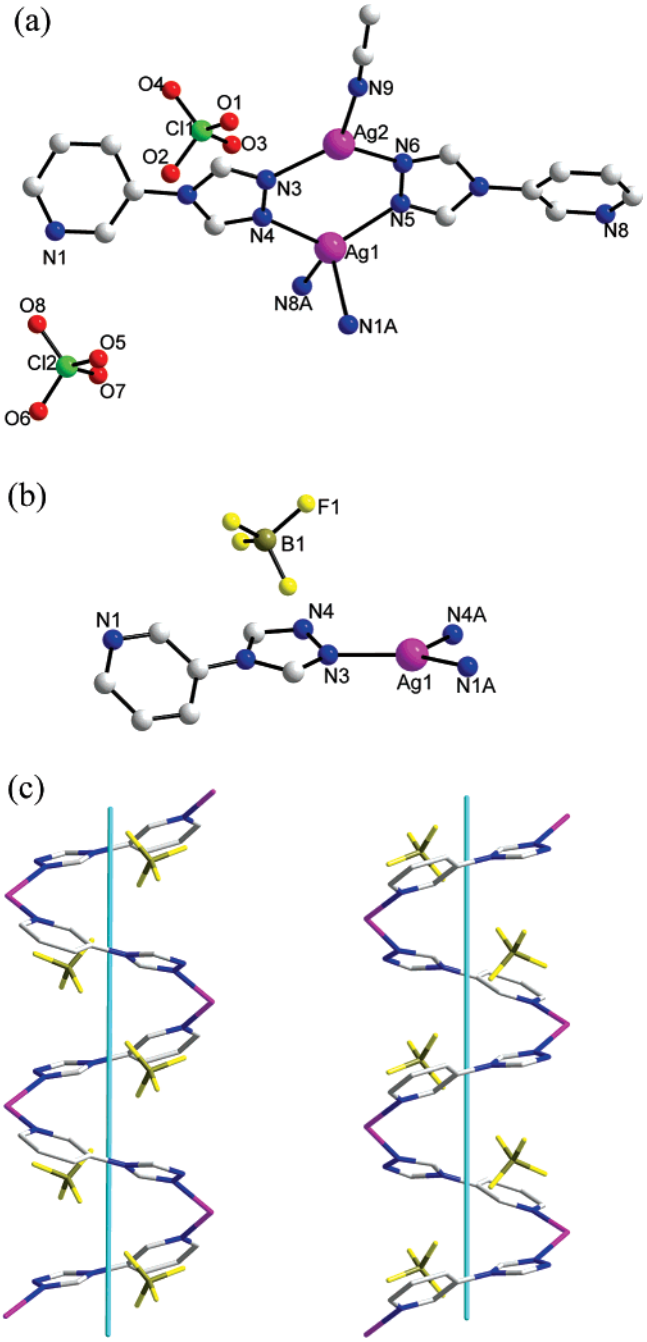

Figure 4. Coordination units of **3a** (a) and **3b** (b) and the left- and right-handed helical chains in **3b** as construction units (c). Color code: purple, Ag; blue, N; gray, C; green, Cl; red, O; brown, B; yellow, F.

acting as the four edges and four Ag^I ions representing the four vertices. All of the Ag^I ions of a layer are coplanar, and no helical chains exist (Figure 7). The NO_3^- anions occupy the space between the neighboring layers.

Structural Analysis of 4. The coordination environment around each Ag^I center in **4** is completed via four $N_{triazole}$ atoms from four distinct μ_4-bridged L_4 ligands (Figure 8). Two Ag^I centers are bridged by four $N_{triazole}$ atoms, giving rise to a dinuclear core $\{Ag_2N_4\}$. Each L_4 ligand in the *ab* plane bridges three Ag^I atoms, and each Ag^I center joins three L_4 ligands to form an infinite 2D-layered architecture with 4.8^2 topology. Although Ag and the ligands in both **3c** and **4** form a 2D network with comparable topologies, **4** has

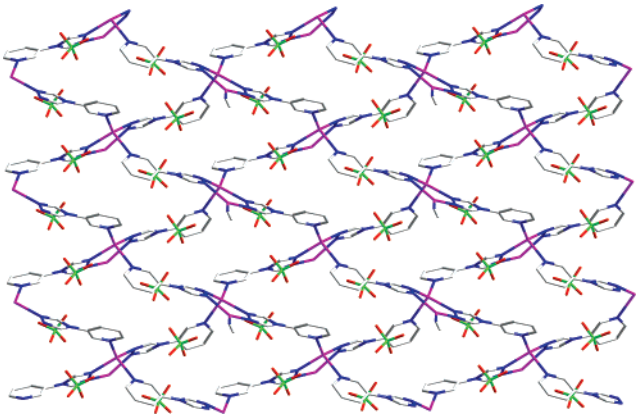

Figure 5. View of a 2D layer in **3a** constructed via helical chains along the *c* axis. Color code: purple, Ag; red, O; green, Cl; gray, C; blue, N.

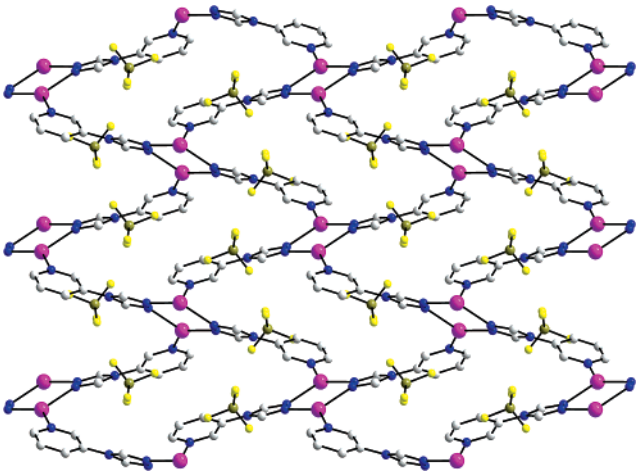

Figure 6. View of a 2D layer in **3b** constructed via helical chains along the *a* axis. Color code: purple, Ag; brown, B; yellow, F; gray, C; blue, N.

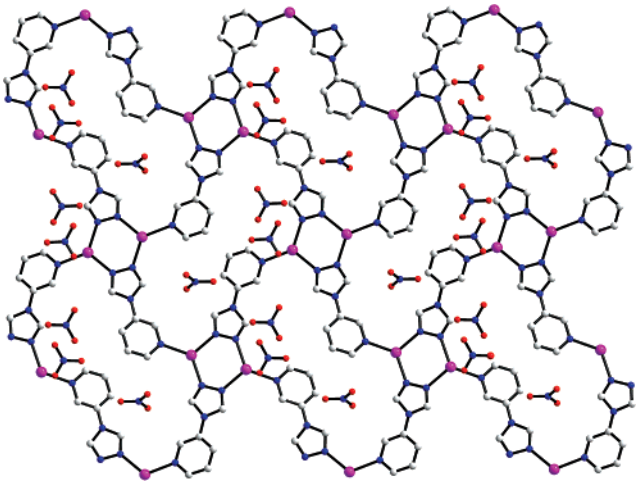

Figure 7. 2D coordination network of **3c** along the *a* axis. Color code: purple, Ag; blue, N; gray, C; red, O.

a 3D grid network with 4.6^3 topology thanks to the higher number of coordination sites of L_4 (see the Supporting Information). As shown in Figure 9, **4** contains a novel porous, noninterpenetrating cationic network with 1D channels parallel to the *a* axis, accepting two columns of uncoordinated ClO_4^- anions filling into every central cavity.

Comparative Study of Self-Assembly Results. Investigations of the self-assembly between silver(I) salts and four

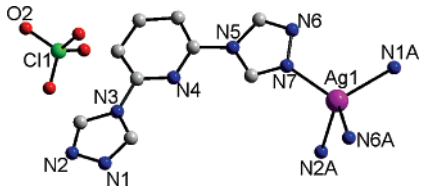

Figure 8. Coordination unit of complex **4**. Color code: purple, Ag; blue, N; gray, C; green, Cl; red, O.

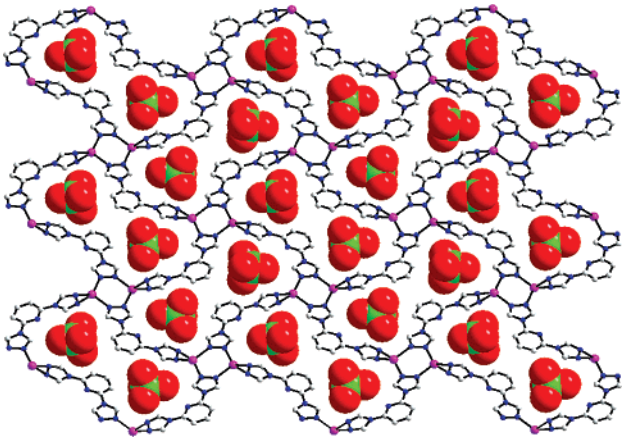

Figure 9. 3D coordination network of complex **4** along the *a* axis. Color code: purple, Ag; blue, N; gray, C; green, Cl; red, O.

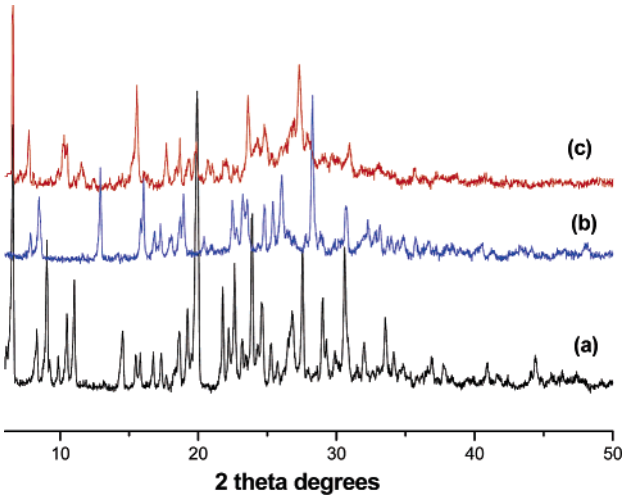

Figure 10. PXRD patterns of the self-assembly products based on L_4 and $AgClO_4$ (a), $AgNO_3$ (b), and $AgBF_4$ (c).

4-substituted 1,2,4-triazole ligands, nine novel crystal products, and two crystalline powders were isolated. The PXRD results of the products based on AgX salts and L_4 are shown in Figure 10. The peak positions in parts a−c are almost the same. The different PXRD patterns of parts a and c imply that the products based on $AgBF_4$ and L_4 may have coordination networks different from those of **4**. The characteristic peaks of the $AgNO_3$ complex are different from those of the original **4**, which indicates that they have different coordination networks probably because NO_3^- anions are involved in the coordination of the Ag^I centers.

The self-assembly of silver(I) salts with bitopic ligands L_1 or L_2 mostly yielded discrete compounds or 1D polymers, such as dinuclear complexes **1a**−**1c**, **2b**, or **2a**, respectively. In order to obtain high-dimensional MOFs, tritopic ligand L_3 was employed and three 2D coordination polymers were

formed. It is interesting to note that counteranion effects influence the configurations of the coordination layers. **3a** contains a right-handed helical network with (4,4) topology; **3b** is a meso layer constructed via left- and right-handed helical chains; **3c** is a 4.8^2 net with no helical chains. Structure analyses show that the pitch of the self-assembled helical spring with various sizes can also be tuned by different anions. In order to obtain 3D complexes, L_4 with more coordination sites than L_1-L_3 was employed and a 4.6^3 network with rhombic channels, accepting two columns of uncoordinated ClO_4^- anions filling into every central cavity, was isolated for **4**. The triazole ligands in the *ab* plane bridge Ag^I ions to form a 2D layer with 4.8^2 topology, which has a configuration similar to that of **3c**. Our results show that the increase of the coordination sites of ligands is an effective route to obtaining higher-dimensional structures. Obviously, the number of coordination sites from 2 to 4 corresponds to the dimensionalities of the complexes from zero to three.

Solid-State and Solution Emission Spectroscopy. The emission spectra for complexes **1a**−**1c**, **2a**, **2b**, and **3a**−**3c** in the solid state are shown in the Supporting Information, and all of the complexes are excited at 383 ± 2 nm. The main emission bands of these complexes are located at almost the same position (λ_{max} = 435 ± 3 nm), exhibiting a strong blue fluorescence with slightly different band shapes. All of the complexes also exhibit some low-energy emission bands, which have shapes and positions similar to those of triazole ligands. The emissions are neither metal-to-ligand charge transfer (MLCT) nor ligand-to-metal charge transfer in nature and probably can be assigned to the intraligand fluorescent emission because very similar emissions are also observed for the free ligands.[13b]

All of the title complexes exhibit broad blue fluorescence in a water solution from blue to green (see the Supporting Information). The maximal emissions are 515 ± 1 nm for **1a**−**1c**, 369 ± 1 nm for **2a** and **2b**, and 406 ± 2 nm for **3a**−**3c**, which are excited at 328 ± 2, 297 ± 2, and 368 ± 2 nm, respectively. The emissions of **1a**−**1c** may be derived from MLCT because the free ligand L_1 is not emissive in water at ambient temperature. The fluorescent emissions of **2a**, **2b**, and **3a**−**3c** are probably assigned to the intraligand fluorescent emission because similar behaviors are also observed for the free L_2 and L_3 ligands in a water solution. Compared with the complexes **2a** and **2b**, the maximum wavelength and the intensity of excitation and emission in **3a**−**3c** are red-shifted and weaker, respectively, both of which are likely due to the more extended π system in **3**.

At ambient temperature, the free ligand L_4 and its complex **4** in a water solution are luminescent and show a broad emission maximum at 515 nm with excitation at 332 and 393 nm, respectively (see the Supporting Information). The chromophores of the ligand are the aromatic rings, and the observed emission is due to the $\pi-\pi^*$ transition. In the solid state, both L_4 and **4** exhibit strong blue emission with λ_{max} = 436 nm, while excitation is at 396 and 385 nm, respectively. Compared with the fluorescent emissions of the free ligand L_4 and its complex **4** in solution, the emissions are blue-shifted and narrow.

The investigation of luminescent properties for four triazole ligands and their Ag^I and Cd^{II} complexes[13b,c,14b] showed that (i) all of the triazole ligands have 4-substituted aromatic rings, which give similar $\pi-\pi^*$ transitions in the solid state, and hence their Ag^I and Cd^{II} complexes in the solid state are found to have very similar behavior in the emission spectra, and (ii) there are no low-energy emission bands observed for the free ligands and their complexes in the solution spectra. Our results show that 1,2,4-triazole derivatives and their Ag^I and Cd^{II} complexes are good choices for potential fluorescent materials.

Conclusion

In summary, as a continued investigation of the coordination chemistry of triazole ligands, a series of novel triazolatesilver(I) luminescent complexes were synthesized. Structural analyses indicate that the increase of coordination sites (from 2 to 4) of the ligands is an effective route to obtaining high-dimensional structures (from zero to three). **1a**−**1c** and **2b** are dinuclear complexes linked by two N1,N2-bridged triazole ligands. **2a** is a unique 1D molecular-ladder complex. The reaction of L_3 with different silver(I) salts afforded a right-handed helical 2D network with (4,4) topology for **3a**, a meso layer constructed via left- and right-handed helical chains for **3b**, and a 2D 4.8^2 net containing no helical chain for **3c**. Using tetratopic ligand L_4, a cationic 4.6^3 network with rhombic channels, accepting two columns of uncoordinated ClO_4^- filling into every central cavity, was isolated for **4**. All of the complexes in the solid state exhibit strong fluorescent emission bands, which may be assigned to the intraligand fluorescent emission. The emissions of these complexes in a water solution varied from blue light to green light at ambient temperature. These results render the title complexes potentially for use as fluorescent materials.

Acknowledgment. We genuinely appreciate the reviewers for giving their invaluable comments. This work was supported by the National Natural Science Foundation of China (Grants 20631030 and 20425103), the NSF of Tianjin (Grant 06YFJZJC009000), the State Key Project of Fundamental Research of MOST (Grant 2005CCA01200), and MOE (Grant 20060055039) of China.

Supporting Information Available: Crystallographic data in CIF format and additional figures. This material is available free of charge via the Internet at http://pubs.acs.org.

IC060855Y